HHS Public Access

Author manuscript

JACC Cardiovasc Imaging. Author manuscript; available in PMC 2016 June 01.

Published in final edited form as:

JACC Cardiovasc Imaging. 2015 June ; 8(6): 710–723. doi:10.1016/j.jcmg.2015.03.005.

Recent Advances in Cardiac Computed Tomography: Dual Energy, Spectral and Molecular CT Imaging

Ibrahim Danad, MD[a], **Zahi A. Fayad, PhD**[b], **Martin J. Willemink, MD**[b,c], and **James K. Min, MD**[a,*]

[a]Department of Radiology, Weill Cornell Medical College, Dalio Institute of Cardiovascular Imaging, NewYork-Presbyterian Hospital, New York, NY, USA [b]Translational and Molecular Imaging Institute, Icahn School of Medicine at Mount Sinai, New York, NY, USA [c]Department of Radiology, University Medical Center Utrecht, The Netherlands

Abstract

Computed tomography (CT) evolved into a powerful diagnostic tool and it is impossible to imagine current clinical practice without CT imaging. Due to its widespread availability, ease of clinical application, superb sensitivity for detection of CAD, and non-invasive nature, CT has become a valuable tool within the armamentarium of the cardiologist. In the last few years, numerous technological advances in CT have occurred—including dual energy CT (DECT), spectral CT and CT-based molecular imaging. By harnessing the advances in technology, cardiac CT has advanced beyond the mere evaluation of coronary stenosis to an imaging modality tool that permits accurate plaque characterization, assessment of myocardial perfusion and even probing of molecular processes that are involved in coronary atherosclerosis. Novel innovations in CT contrast agents and pre-clinical spectral CT devices have paved the way for CT-based molecular imaging.

Keywords

Dual-energy CT; spectral CT; molecular CT imaging

Corresponding author: James K. Min, MD, Weill Cornell Medical College, NewYork-Presbyterian Hospital, Dalio Institute of Cardiovascular Imaging, 413 E. 69th Street, Suite 108, New York, New York 10021, 646-962-6192, jkm2001@med.cornell.edu.

Disclosures

Ibrahim Danad: None
Zahi A. Fayad: None
Martin J. Willemink: None
James K. Min: Consultant / Scientific Advisory Board: Arineta, Abbott Vascular, Myokardia, CardioDx.

INTRODUCTION

Since the advent of 64-detector row computed tomography (CT) in 2005, coronary CT angiography (CCTA) has been demonstrated as a promising non-invasive technique for evaluation of coronary artery stenosis (1,2). In the last few years, numerous technological advances in CT have occurred—including dual energy CT (DECT), spectral CT and CT-based molecular imaging. Early studies of these methods have been largely promising and showed improved cardiac and coronary evaluation. An understanding of these advanced CT principles is required to fully appreciate the promise of the applicability of these technologies for the evaluation of individuals with cardiac and coronary disease.

The Principles of Dual Energy Computed Tomography

Improvements in CT, while rapid in recent years, are nevertheless constrained by the physical principles underlying this technology that are a function of x-ray attenuation detected from multiple orientations around an imaged object. From a basic sense, these principles are generally two-fold, and include the photoelectric and Compton effects when considering x-ray photons within the diagnostic energy range (Figure 1). The former is highly dependent on the photon energy level and is related to the atomic number and photon energy level, whereas the latter is independent of the photon energy level but rather related to material density. For proper grasp of the advances in dual energy and spectral CT, a basic understanding of these principles is required.

The photoelectric effect is the ejection of an electron from the innermost shell of an atom (K-shell) by a photon with a greater energy than the binding energy of the K-shell. As a result, the total energy of any incoming photon is absorbed (Figure 1). The binding energy of electrons in the K-shell is material specific and is proportional to the atomic number (Z). For a given photon energy, the photoelectric effect scales on a magnitude order of Z^3. However, this does not imply that an element with Z = 100 yields an 8 times greater attenuation than a material with Z = 50. This can be explained by the spike in attenuation seen related to a maximal photoelectric effect (the K-edge), this occurs when the photon energy levels is just greater than the electron binding energy of the K-shell of an atom. The K-edge value varies for each material and is higher with increasing atomic numbers. Paradoxically, the photoelectric effect is maximal at K-edge of the absorber and is reduced with increasing photon energy levels, inversely proportional to the photon energy cubed ($1/E^3$). Therefore, the probability of the photoelectric effect is dependent on both the atomic number and the photon energy level according to Z^3/E^3.

The Compton effect is the collision of photons with valence electrons of the outermost shell of an atom. In contrast to the photoelectric effect, the energy of the incoming photon is not totally absorbed giving rise to photon scattering (Figure 1). Compton scattering is dependent on the density of electrons and since all elements have approximately the same amount of electrons per unit mass, the atomic number is of less relevance for the occurrence of Compton scattering. Dual-energy CT principles are largely based on the photoelectric effect and can be achieved by exploiting the energy dependent attenuation of materials when exposed to two different photon energy levels. These physical principles can be exploited

for *in vivo* human imaging, as DECT is based on dissimilar tissue characteristics with respect to their energy-dependent x-ray attenuation. Subsequently, DECT enables the distinct differentiation between two basis materials (Figure 2). These materials can be chosen arbitrarily, as long as their K-edges are sufficiently different (i.e. attenuation profiles), such as water and iodine. Any other material with an attenuation spectrum different than that of the chosen basis materials will be reflected as a combination of the two basis materials (Figure 3). As such, exploiting differences in energy-related attenuation of tissues, DECT provides information about tissue composition that is unobtainable with conventional single-energy CT (SECT).

The advantage of using different energy x-ray levels for decomposition of tissues has been known for a long time and was even mentioned by Hounsfield in his original paper on CT four decades ago: "*Two pictures are taken of the same slice, one at 100 kV and the other at 140 kV so that areas of high atomic numbers can be enhanced. Tests carried out to date have shown that iodine (Z = 53) can be readily distinguished from calcium (Z = 20)* (3)." However, this approach at that time was suffering from technological limitations and was therefore abandoned.

Dual Energy CT Methods

While SECT imaging is typically performed with polychromatic energy levels of photons set to 120 or 140 kVp, energy levels of photons with DECT are typically 80 and 140 kVp for the acquisition of low and high-energy dependent tissue attenuation profiles, respectively. The exploitation of two polychromatic energy spectra by DECT can be achieved by at least 3 different methods (Figure 4): 1) two x-ray source and detector pairs with each source operating at a different tube voltage; 2) a single source-detector pair with an x-ray tube capable of rapidly switching between low and high tube potential or by switching tube potential between gantry positions; and 3) an x-ray source operating at constant tube voltage with a double-layer detector capable of differentiating between low and high-energy photons.

Clinical Applications of Dual-energy CT: Myocardial Perfusion Imaging

As compared to SECT, DECT may allow for better tissue characterization and therefore enhanced visualization of myocardial perfusion defects and thus, encourage its use for ischemia assessment. Given the unique feature of DECT to allow for differentiation of iodine attenuation characteristics when it is exposed to different photon energy levels, DECT allows for the mapping of iodine distribution in the myocardium as a quantitative, albeit surrogate, marker for perfusion and blood volume (4) (Figure 5). There is an early body of evidence showing the clinical feasibility of a DECT myocardial perfusion protocol as a supplement to CCTA anatomic evaluation of the coronary arteries (5–7). The majority of these investigations have compared DECT to rest-stress SPECT, cardiac MRI (CMR) or invasive coronary angiography (ICA) as reference standard (5,7–11). In a small study (n = 20) by Weininger et al., stress-rest first-pass myocardial perfusion DECT ($DEFP_{CT}$) detected myocardial perfusion defects on CMR with a sensitivity and specificity of 93% and 99%, respectively (12). Also against a CMR reference standard, Ko and colleagues found

that stress-rest $DEFP_{CT}$ could detect reversible perfusion defects with a sensitivity and specificity of 89% and 78%, respectively (9). While $DEFP_{CT}$ alone revealed the diagnosis of ischemia corresponding to a ≥ 50% stenosis on ICA with a sensitivity of 89% and specificity of 76% (9), it is conjectured that a hybrid approach—namely combining DECT perfusion with CCTA—may enhance the diagnostic accuracy of physiologic coronary artery disease assessment through improvements in specificity (13).

In this regard, three studies have demonstrated the incremental diagnostic value of combining DECT myocardial perfusion imaging (MPI) with CCTA (6,10). Ko et al showed that the addition of DECT perfusion to CCTA resulted in an improvement of sensitivity, specificity, negative predictive value and positive predictive value from 91.8%, 67.7%, 87.7%, and 73.6% to 93.2%, 85.5%, 91.4% and 88.3%, respectively (6). While Wang and colleagues found no differences in sensitivity and negative predictive value (both remained 100%), they reported specificity to significantly improve from 37.5% to 75% by the combination of DECT perfusion imaging with CCTA (10). A recently published study confirmed the incremental value of DECT perfusion imaging as an adjunct to CCTA, which decreased the number of false-positive CCTA results as reflected by an improvement in both specificity and positive predictive value, 56% to 79% and 55% to 71%, respectively. As a consequence, the hybrid approach improved accuracy significantly from 69% to 82% (14).

These results suggest that DECT MPI may decrease the number of false-positive CCTAs, which is in line with the observations seen for hybrid positron emission tomography and SPECT/CCTA studies (15). Despite the notion that combined physiologic-anatomic evaluation by DECTP, a study by Wang and colleagues observed a negligible effect of DECT MPI when added to CCTA for measures of diagnostic accuracy, with a compromised increase in sensitivity from 82% to 90% at the loss of specificity (91% to 86%) (5). Similarly, a recently published pilot-study reported DECT MPI to improve accuracy of CCTA alone, however, the combination of these two tests resulted in a lower performance compared to DECT perfusion imaging alone (16). Several important considerations of DECT MPI imaging have been discussed, and require attention for optimization of MPI protocols. Among the early studies of DECT MPI, there has been variability of when to perform the “rest” portion versus the “stress” portion, with many contending that vasodilator stress is important to perform first to reduce the chance of residual contrast that may confound perfusion defects. In contrast, others have argued for a rest-first protocol, maintaining the importance of coronary artery evaluation by CCTA as the foremost information to be garnered from the study. Pertaining to the latter, rest DECT has been reported to allow for detection of perfusion defects not visible at rest SPECT imaging (5,11), and suggests it as a possible adjunct to traditional CCTA evaluation. This finding may be due to a myriad of reasons, including the higher spatial resolution of CT that may encourage the detection of subtle perfusion abnormalities that are not visible on SPECT (5,11,17). However, a recent study by Ko and colleagues reported stress DECT MPI to convey a higher accuracy for the detection of ischemia compared to rest DECT perfusion imaging (14). Despite these early studies that emphasize the potential of DECT to provide complementary information on coronary artery disease, DECT MPI may be regarded as being in its infancy, with published studies to date limited by small sample sizes, referral bias and the lack of a proper reference standard.

Clinical Applications of Dual-energy CT: Coronary Atherosclerotic Plaque Characterization

From prior invasive and pathologic evaluations, several coronary atherosclerotic plaque features have been implicated as crucial to the pathogenesis of acute coronary syndromes, and include measures of plaque burden, thin cap fibroatheroma, inflammatory infiltration, intraplaque hemorrhage, micro calcifications and a necrotic lipid-rich core (18–20). Given their importance, these plaque features have been extensively investigated by SECT, given the relative ease with which SECT can reliably separate calcified and non-calcified plaques. Yet conventional CT faces a significant challenge in differentiating different components of non-calcified plaques (e.g., lipid-rich versus fibrous). Several studies showed considerable overlap in Hounsfield units between lipid-rich and fibrous-rich non-calcified plaques inherent to the spatial resolution of CT and a variable intra-plaque uptake of iodine contrast agents (21–23).

It has been posited that DECT may overcome these limitations owing to its capability of tissue decomposition, although early results have been mixed. CT-attenuation based characterization of non-calcified plaques using DECT has been examined by an *ex vivo* study of 15 human arteries, with discriminatory improvement with DECT over conventional SECT (24). In contrast, in a small prospective study of individuals undergoing IVUS and CT, DECT had an almost similar sensitivity compared to SECT (45% versus 39%, respectively) for necrotic core detection (25). Even when using post-mortem samples wherein image quality is not governed by body habitus or motion, DECT misclassified 21% of non-calcified plaques (26).

The mixed findings observed to date may be due to an array of issues, including scanning protocols as well as DECT image visualization. As indicated above, DECT may allow for both monochromatic energy imaging as well as material basis decomposition. To date, the exact energy and/or material basis pair that optimize plaque visualization have not been systematically evaluated. Future studies will be required to determine the proper methods for plaque characterization by this emerging technology.

Minimizing Image Artifacts using Dual-energy CT

Image quality is particularly challenging when it comes to a moving organ such as the heart. Sufficient diagnostic image quality is highly dependent on patient's heart rate. Therefore, heart rate control is mandatory when performing CT-based coronary angiography. Alternatively, dual-source CT is less susceptible to artifacts as a result of high or irregular heart rates due to its high temporal resolution. Scheffel et al demonstrated dual-source CT to provide high diagnostic accuracy for the detection of CAD in patients with extensive calcifications (50% had an Agatston score > 400) and without heart rate control, a population that is often considered challenging for conventional CCTA (27). Additionally, in a recent meta-analysis dual-source CT in patients with atrial fibrillation yielded similar diagnostic value as standard CCTA in patients with stable and regular heart rates (28). The improved performance of dual-source CT in this specific population is attributable to the high temporal resolution of dual-source CT (66 – 75 ms) that allows for less motion artifacts

to occur (28). Further, the unique features of the DECT dataset allows for the generation of virtual monochromatic images, which are analogous to conventional SECT images. Albeit, monochromatic images depict a scanned object at a single X-ray energy level, rendering these images less susceptible to beam-hardening and blooming artifacts (29–31). Due to the polychromatic nature of the x-rays used in conventional CT, imaging of high-density objects will result in substantial absorption of lower energy photons giving rise to a shift towards a high-energy x-ray beam. This alteration of the photon-energy spectrum leads to distortions in the reconstructed image of high-attenuation tissue or objects such as, amongst others, coronary stents, high concentrated contrast and/or calcium. Indeed, coronary calcifications and metal artifacts from coronary stents are known for hampering the diagnostic value of CT-based coronary artery imaging. Interestingly, monochromatic images at high-energy levels suffer less from blooming and beam-hardening artifacts. Therefore, analyzing mono-energetic high-energy images carries with it the potential to reduce these artifacts (32). It has been demonstrated that calcium blooming and beam-hardening artifacts that impair accurate delineation of stenosis degree are significantly reduced at high-energy levels using phantom models (33,34). Another phantom study showed improved enhancement of coronary stent lumen, beyond that achieved with traditional CT, using DECT technology based on a dual-layer detector (33). A recently published feasibility study performed in 21 patients, revealed that single-source DECT (rapid kV switching) with monochromatic image reconstructions below 80 keV were associated with an increase in stent-related blooming artifacts, causing an underestimation of stent diameter (35). Similarly, Secchi et al evaluated artifact size in 35 patients and reported substantial reductions of high-attenuation artifacts, resulting from metal artifacts (coronary stents, bypass clips, and sternal wires) and concentrated contrast in the vena cava, by using monochromatic images at high energy levels (36). With stress myocardial perfusion CT, beam-hardening arising from high-density iodinated contrast hampers accurate assessment of myocardial perfusion. Studies using ex vivo hearts and phantom models demonstrated improved detection of myocardial perfusion defects by reduction of beam-hardening artifacts mimicking perfusion deficits using fast-switching kVp DECT technology (37,38). A clinical study by So et al showed rapid kV-switching projection-based DECT to improve ischemia detection by elimination of beam-hardening artifacts (4). Notably, DECT data obtained with a rapid kV-switching DECT device allows for the generation of monochromatic images from projection-space, theoretically providing a more sophisticated beam-hardening correction over the image-based method (38–40). However, clinical studies on this topic are currently lacking.

Radiation Dose Aspects of Dual-energy CT

Despite the fact that cardiac CT provides invaluable information regarding diagnosis and patient management of patients evaluated for CAD, the exposure to ionizing radiation is of concern with CT-based imaging. In recent years, substantial reductions in radiation dose have been achieved with the implementation of ECG-guided tube modulation, prospective-ECG gated imaging (step-and-shoot mode), and body-mass-index based tube voltage reductions. As a consequence, dose reductions by more than 60%, and even 90% in some studies, have been achieved without a sacrifice in both image quality and diagnostic performance (41–44). Nevertheless, the question rises whether cardiac imaging using dual-

energy CT comes with a radiation dose penalty as compared to SECT. In an early small clinical study, dual-source CT in single-energy mode (4.54 ± 1.87 mSv) and DECT (9.8 ± 4.77) were shown to deliver less radiation than regular 16–slice multi-detector CCTA (12 ± 3.59 mSv) in a routine clinical setting in patients with low and stable heart rates (45). Halliburton and colleagues compared in a clinical setting dual-source and 32-slice CT with regard to radiation exposure, and they showed no difference in radiation doses for coronary imaging between the two modalities (46). Similarly, in a head-to-head prospective randomized clinical trial evaluating 102 patients, DECT based on rapid-kV-switching enabled coronary CTA examinations at dosage levels comparable with contemporary multi-detector CCTA, 2.31 vs. 2.23 mSv, respectively (47). Although no study has evaluated the radiation dose of DECT devices based on double-layer technology for cardiac imaging, presumably these devices will produce similar radiation doses overall to single-energy CT, since there is no double irradiation of tissue to obtain low and high-energy datasets. However, these data are acquired at 140 kVp, which is a high tube potential for most cardiac imaging. Arguably, lowering tube current will balance the effects of high tube voltage imaging without impacting spectral separation, but data are to date lacking.

Radiation dose in cardiac CT is closely related to the pitch value, whereby a pitch value < 1 implies overlapping image slices (table movement is less than one detector width during one gantry rotation) and a pitch greater than 1 indicates gaps between radiation beams. Interestingly, dual-source CT systems have enabled the implementation of high-pitch spiral acquisition protocols with pitch values of 3.0 and higher, avoiding overlapping radiation exposure, allowing for shorter scan times, and thus reducing effective radiation dose (48–50). Notably, high-pitch spiral acquisition are only possible with dual-source CT owing to its unique geometry of a dual-source detector pair providing, amongst others, a high temporal resolution by utilizing only a quarter of the gantry rotation time to obtain one cross-sectional image. The tube-detector pair allows for fast table movement, whereby image gaps in the trajectory of the first detector are covered by the second detector. As such, the dual-source high-pitch mode allows coverage of the entire heart in the diastolic phase of one cardiac cycle, which is referred to as prospective ECG-gated spiral scanning. This approach has markedly reduced radiation doses to sub-millisievert fractions, albeit in single-energy mode (48–56). Clinical feasibility studies investigated the diagnostic accuracy of high-pitch protocols and found that CT-based coronary angiography could be performed with effective radiation doses averaging 1 mSv, without a penalty in terms of diagnostic accuracy and image quality (48–56). Although high-pitch scanning holds great promise, a drawback of this mode is that the image data of the entire heart needs to be acquired during the diastasis of one heartbeat. Consequently, with the second-generation dual-source devices (acquisition speed 458 mm/s and temporal resolution of 75 ms at a gantry rotation time of 282 ms) coverage of the entire heart (≈ 12 cm) requires typically 250 ms. Therefore, the high-pitch mode is only restricted to patients with a low (< 65 bpm) and regular hear rate in order to match the required long image acquisition window (48–52,55). Recently, pilot-studies demonstrated the feasibility of high-pitch coronary examinations using third generation dual-source CT devices (acquisition speed 737 mm/s and a temporal resolution 66 ms owing to a gantry rotation time of 250 ms) to obtain good quality images at heart rates up to 75 bpm with sub-millisievert radiation dose (53,56).

Notably, the achieved sub-millisievert radiation doses were achieved via a combination of multiple dose saving strategies such as prospective ECG-triggering, low tube voltages and iterative image reconstructions. The increased image noise resulting from low voltage imaging is offset by the application of iterative reconstruction techniques (54,57,58). These novel reconstruction algorithms have reduced image noise derived from low-photon counting, while increasing image quality. A recently published small-scaled clinical study of 26 patients, revealed effective radiation doses to be 0.3 mSv using a third generation dual-source device capable of producing a high tube current at a tube voltage of 70 kVp without a sacrifice in image quality, albeit in a selected body weight population (<100 kg) with low heart rates (54). Similarly, Schuhbaeck and colleagues managed to reduce effective radiation dose below 0.1 mSv in 21 patients using a high-pitch spiral acquisition mode with low tube voltage (80 kVp) in conjunction with low tube voltage and iterative image reconstruction (57). In addition, diagnostic performance of sub-millisievert CCTA examinations is high, using ICA as a reference, despite the low radiation dose delivered to patients (59). By harnessing the advantages of dual-source CT devices combined with low voltage imaging and iterative image reconstructions, radiation dose of a coronary CT study is only a fraction of 1 mSv, which is comparable to the dose of a mammogram (0.4 mSv).

Another application of DECT for further radiation dose reduction is the generation of virtual unenhanced (VUE) images through the utilization of post-imaging reconstructions that are unique to DECT. These VUE images are generated from contrast-enhanced scans by virtual iodine subtraction using three-material decomposition algorithms and may replace true contrast-enhanced scans (60,61). Subsequently, coronary artery calcium (CAC) scoring and a standard contrast CCTA can all be gleaned from one single scan, obviating the need for a separate non-contrast CAC-scoring CT. In this way, scan acquisition time, costs and radiation to the patient may be decreased. Several studies already demonstrated the feasibility of CAC-scoring on VUE by showing a good agreement of the CAC-score derived from VUE with true non-contrast CAC-score scans. Yamada et al revealed that DECT coronary angiography using VUE for calcium scoring resulted in a 20% dose reduction compared to conventional CCTA with a prior separate non-contrast CAC scan (62), while in a recently published study an average dose reduction of 51% was seen by replacing separate CAC-score scans by VUE imaging for quantification of coronary calcium deposits (63). Although promising, the technique is still in its infancy and further validation and more sophisticated correction algorithms are warranted to avoid underestimation of CAC burden by incorrect subtraction of calcium content mimicking iodine contrast agents.

Iodinated-contrast Dose Requirements

Contrast-enhanced CT imaging bears the risk of inducing an acute deterioration in renal function, particularly in patients with pre-existing kidney disease. Although the incidence of contrast-induced nephropathy is low, it is associated with significant morbidity and even death (64). However, lowering contrast volume comes at the cost of lower image quality due to impaired contrast-to-noise and signal-to-noise (65). Nonetheless, previous studies observed increased conspicuity of iodine-based contrast agents achieved with low tube voltage, while facilitating reduction of iodine load and radiation dose (30,66,67). In a recent study, Scheske et al reported improved signal-to-noise and contrast-to-noise ratios in both

the myocardium and coronary arteries with low-energy monochromatic imaging as compared with polychromatic CT (29). Therefore, an optimal difference in contrast attenuation between normally perfused myocardium (high attenuation) and ischemic myocardium is anticipated with low-energy monochromatic imaging, considering the low K-edge of iodine. In a prospective randomized clinical study of 102 patients, Raju et al evaluated the feasibility of DECT associated with reduced iodine load, and they found that monochromatic images at 60 keV provided signal- and contrast-to-noise ratios comparable to SECT coronary angiography with full iodine load, while preserving diagnostic interpretability (47). Interestingly, this was accomplished despite a more than 50% reduction in iodine load for CT angiography with DECT. Similarly, a recently published study revealed that monochromatic images at 50–60 keV allow for a iodine volume reduction up to 60% without compromising image quality as reflected by similar contrast- and signal-to-noise ratios as those obtained with standard CCTA using full iodine load (68).

CT-based Molecular Imaging: Nanoparticle Contrast Agents

Iodinated contrast and barium suspensions are currently the only approved CT contrast agents, and are employed for their ability to enhance visualization by increased attenuation of x-ray photons. Recently, nanoparticle contrast agents—tiny particles within the range of 1 to 100 nm—have received considerable interest (Figure 6). Several of these nanoparticles have been approved for therapeutic and diagnostic applications in the field of oncology (69,70). This is due to a number of reasons, including longer circulatory half-lives obviating the need for repeated injections, and modifiable properties that offer tissue specificity (71–76).

One of the nanoparticle CT contrast agents with promising preliminary results is compound N1177. This is a suspension composed of crystalline iodinated particles dispersed with surfactant and has high affinity for activated macrophages (77). Upon injection, increased densities of N1177 contrast are detectable in atherosclerotic plaques that correspond to macrophage infiltration in post-mortem samples (77). Referenced against a histopathologic reference standard, N1177 demonstrates high affinity to aortic atherosclerosis in animal models, and high correlation to FDG-uptake, a known surrogate marker for macrophage density (78). In a related study by Cormode et al, a gold-core high-density lipoprotein particle targeted at macrophages was found to accumulate in atherosclerotic plaques in aorta walls of a mouse model as detected by microCT (76). Rabin and colleagues developed a long circulating bismuth sulphide nanoparticle agent for CT (79). X-ray absorption was fivefold better than iodine, circulation times were longer than 2 hours in vivo and the efficacy and safety profile was comparable or better than iodinated contrast agents (79). Pan et al evaluated another heavy metal called Ytterbium, which was developed to complement spectral CT (80). The specific goal of these particles would be detection of non-occlusive micro thrombus associated ruptured plaques within the coronary arteries. It is notable to mention, however, that these encouraging findings have been validated in animal studies alone, with human evaluation currently lacking.

Spectral CT imaging

Similar to DECT, spectral CT—often referred to as “multicolor CT”—exploits the energy dependent attenuation of x-ray photons, and may be coupled to nanoparticles to potentially offer improved atherosclerosis evaluation. In contrast to DECT, which is performed with only two photon energy levels, spectral CT utilizes multiple energy levels to provide more detailed tissue information based upon their behavior at different x-ray spectra (information that is disguised by the usage of only two x-ray spectra). The principle of spectral CT relies on an energy sensitive photon counting detector that enables differentiation of photons from multiple energy levels. In this configuration, when a photon collides with an x-ray detector, a current pulse is generated proportional to the energy of the detected x-ray photon. Subsequently, the detected photon is allocated to energy bins representing several electron voltage intervals. A specific element can be more easily detected with the limits of the bins placed at the K-edge of the material of interest. As such, simultaneous sampling of multiple photon energy levels allows for a more sophisticated characterization of tissues based on K-edge behavior of multiple materials. To date, only pre-clinical data based on phantom models and post-mortem samples are available on coronary plaque imaging using photon-counting CT devices. Nevertheless, this technique holds great potential allowing for the precise detection and quantification of contrast agents and enables its extraction and separation from tissue components (81). Different approaches for spectral CT are being developed. One of those is the MARS CT scanner that incorporates a MARS camera with a Medipix3 spectroscopic photon counting detector (82). A single polychromatic x-ray tube is used in this system with an energy discriminating photon counting detector with selectable thresholds (83). So far, these scanners are used in the pre-clinical setting. DxRay developed another photon counting detector that was evaluated on a LightSpeed VCT scanner (GE Healthcare, Waukesha, WI, USA). This detector is based on cadmium telluride and cadmium zinc telluride arrays (84). In vivo patient CT images were acquired and the spectral technique was used to remove calcium from the images, resulting in a good image quality (84). Siemens Healthcare developed another approach, a prototype scanner with a photon counting technique implemented in the context of a clinical CT system (85). This prototype system is equipped with both a cadmium telluride photon counting detector and a conventional detector from a clinical CT scanner. Using both approaches allows for direct comparison of image quality between photon counting and conventional detectors. A chess pattern configuration for energy level thresholds enables a virtual number of four energy bins. Image acquisition of an anatomical phantom demonstrated increased Iodine contrast allowing for a potential radiation dose reduction up to 32%. Finally, Philips Healthcare developed a preclinical spectral CT scanner (86). This animal CT system is equipped with a single-line photon counting cadmium telluride array that allows for measurements of six energy bins (87). Feuerlein and colleagues reported that this preclinical spectral CT system improved coronary luminal depiction by effectively isolating gadolinium agents from contrast-free calcified plaques and stent material using a phantom model (87). A recently published study by Boussel et al is the first study, albeit in vitro, about human coronary plaque analysis with the preclinical photon counting spectral CT system (88). They reported promising results regarding its capability to differentiate distinct coronary plaque components based on differences in spectral attenuation and iodine-based contrast

concentrations. Of note, the absorption of low-energy photons by the human body renders the use of K-edge imaging with iodine challenging given its low K-edge energy of 33.2 keV. Therefore, to harness the full benefits of K-edge imaging using photon-counting CT, contrast materials with higher K-edges such as gadolinium (50.2 keV), gold (80.6 keV), and bismuth (90.5 keV), are preferable (Figure 7). However, the potential toxicity of these agents limits their use in humans. Nevertheless, the potential application of gold-based targeted nanoparticles in combination with spectral CT to improve tissue differentiation at the cellular level, albeit in phantom and animal models, has been explored. In a phantom study, Cormode and colleagues demonstrated the feasibility and accuracy of the preclinical spectral CT scanner to simultaneously distinguish between iodine and gold-based contrast agents, tissue and calcifications (75). In addition, the authors showed in an animal model the potential of this preclinical spectral CT system for imaging intra-plaque inflammation using targeted gold-labeled high-density lipoproteins targeting activated macrophages (75). These preliminary results illustrate the potential of CT based molecular imaging using spectral CT in conjunction with nanoparticle contrast agents, to provide valuable information on coronary atherosclerosis anatomy while providing important physiologic data at molecular and cellular level.

Conclusion

In recent years, there have been rapid advances in cardiac CT technology, with progression of conventional SECT to DECT, spectral CT and CT-based molecular imaging. Initial studies of these technologies have been promising, and suggest their potential for improved cardiac and coronary atherosclerosis evaluation.

Acknowledgments

Research funding: This manuscript was funded, in part, by grants from the National Heart Lung and Blood Institute (R01 HL111141, R01 HL115150 and R01 HL118019), as well as from a generous gift from the Dalio Foundation.

List of abbreviations

CAD	coronary artery disease
CCTA	coronary computed tomography angiography
CT	computed tomography
DECT	dual-energy computed tomography
DEFPct	first-pass myocardial perfusion DECT
ICA	invasive coronary angiography
MPI	myocardial perfusion imaging
SECT	single-energy computed tomography
SPECT	single photon emission computed tomography
VUE	virtual unenhanced

References

1. Budoff MJ, Dowe D, Jollis JG, et al. Diagnostic performance of 64-multidetector row coronary computed tomographic angiography for evaluation of coronary artery stenosis in individuals without known coronary artery disease: results from the prospective multicenter ACCURACY (Assessment by Coronary Computed Tomographic Angiography of Individuals Undergoing Invasive Coronary Angiography) trial. Journal of the American College of Cardiology. 2008; 52:1724–32. [PubMed: 19007693]
2. Miller JM, Rochitte CE, Dewey M, et al. Diagnostic performance of coronary angiography by 64-row CT. The New England journal of medicine. 2008; 359:2324–36. [PubMed: 19038879]
3. Hounsfield GN. Computerized transverse axial scanning (tomography). 1. Description of system. The British journal of radiology. 1973; 46:1016–22. [PubMed: 4757352]
4. So A, Hsieh J, Narayanan S, et al. Dual-energy CT and its potential use for quantitative myocardial CT perfusion. Journal of cardiovascular computed tomography. 2012; 6:308–17. [PubMed: 23040537]
5. Wang R, Yu W, Wang Y, et al. Incremental value of dual-energy CT to coronary CT angiography for the detection of significant coronary stenosis: comparison with quantitative coronary angiography and single photon emission computed tomography. The international journal of cardiovascular imaging. 2011; 27:647–56. [PubMed: 21547377]
6. Ko SM, Choi JW, Hwang HK, Song MG, Shin JK, Chee HK. Diagnostic performance of combined noninvasive anatomic and functional assessment with dual-source CT and adenosine-induced stress dual-energy CT for detection of significant coronary stenosis. AJR American journal of roentgenology. 2012; 198:512–20. [PubMed: 22357990]
7. Blankstein R, Shturman LD, Rogers IS, et al. Adenosine-induced stress myocardial perfusion imaging using dual-source cardiac computed tomography. Journal of the American College of Cardiology. 2009; 54:1072–84. [PubMed: 19744616]
8. Meyer M, Nance JW Jr, Schoepf UJ, et al. Cost-effectiveness of substituting dual-energy CT for SPECT in the assessment of myocardial perfusion for the workup of coronary artery disease. European journal of radiology. 2012; 81:3719–25. [PubMed: 21277132]
9. Ko SM, Choi JW, Song MG, et al. Myocardial perfusion imaging using adenosine-induced stress dual-energy computed tomography of the heart: comparison with cardiac magnetic resonance imaging and conventional coronary angiography. European radiology. 2011; 21:26–35. [PubMed: 20658242]
10. Wang Y, Qin L, Shi X, et al. Adenosine-stress dynamic myocardial perfusion imaging with second-generation dual-source CT: comparison with conventional catheter coronary angiography and SPECT nuclear myocardial perfusion imaging. AJR American journal of roentgenology. 2012; 198:521–9. [PubMed: 22357991]
11. Ruzsics B, Schwarz F, Schoepf UJ, et al. Comparison of dual-energy computed tomography of the heart with single photon emission computed tomography for assessment of coronary artery stenosis and of the myocardial blood supply. The American journal of cardiology. 2009; 104:318–26. [PubMed: 19616661]
12. Weininger M, Schoepf UJ, Ramachandra A, et al. Adenosine-stress dynamic real-time myocardial perfusion CT and adenosine-stress first-pass dual-energy myocardial perfusion CT for the assessment of acute chest pain: initial results. European journal of radiology. 2012; 81:3703–10. [PubMed: 21194865]
13. Danad I, Raijmakers PG, Appelman YE, et al. Quantitative relationship between coronary artery calcium score and hyperemic myocardial blood flow as assessed by hybrid 15O-water PET/CT imaging in patients evaluated for coronary artery disease. Journal of nuclear cardiology : official publication of the American Society of Nuclear Cardiology. 2012; 19:256–64. [PubMed: 22076826]
14. Ko SM, Park JH, Hwang HK, Song MG. Direct comparison of stress- and rest-dual-energy computed tomography for detection of myocardial perfusion defect. The international journal of cardiovascular imaging. 2014; 30 (Suppl 1):41–53. [PubMed: 24696012]

15. Danad I, Raijmakers PG, Knaapen P. Diagnosing coronary artery disease with hybrid PET/CT: it takes two to tango. Journal of nuclear cardiology : official publication of the American Society of Nuclear Cardiology. 2013; 20:874–90. [PubMed: 23842709]
16. Carrascosa PM, Deviggiano A, Capunay C, et al. Incremental value of myocardial perfusion over coronary angiography by spectral computed tomography in patients with intermediate to high likelihood of coronary artery disease. European journal of radiology. 2015
17. Meinel FG, De Cecco CN, Schoepf UJ, et al. First-arterial-pass dual-energy CT for assessment of myocardial blood supply: do we need rest, stress, and delayed acquisition? Comparison with SPECT Radiology. 2014; 270:708–16.
18. Finn AV, Nakano M, Narula J, Kolodgie FD, Virmani R. Concept of vulnerable/unstable plaque. Arteriosclerosis, thrombosis, and vascular biology. 2010; 30:1282–92.
19. Naghavi M, Libby P, Falk E, et al. From vulnerable plaque to vulnerable patient: a call for new definitions and risk assessment strategies: Part II. Circulation. 2003; 108:1772–8. [PubMed: 14557340]
20. Naghavi M, Libby P, Falk E, et al. From vulnerable plaque to vulnerable patient: a call for new definitions and risk assessment strategies: Part I. Circulation. 2003; 108:1664–72. [PubMed: 14530185]
21. Petranovic M, Soni A, Bezzera H, et al. Assessment of nonstenotic coronary lesions by 64-slice multidetector computed tomography in comparison to intravascular ultrasound: evaluation of nonculprit coronary lesions. Journal of cardiovascular computed tomography. 2009; 3:24–31. [PubMed: 19201374]
22. Leber AW, Knez A, Becker A, et al. Accuracy of multidetector spiral computed tomography in identifying and differentiating the composition of coronary atherosclerotic plaques: a comparative study with intracoronary ultrasound. Journal of the American College of Cardiology. 2004; 43:1241–7. [PubMed: 15063437]
23. Pohle K, Achenbach S, Macneill B, et al. Characterization of non-calcified coronary atherosclerotic plaque by multi-detector row CT: comparison to IVUS. Atherosclerosis. 2007; 190:174–80. [PubMed: 16494883]
24. Tanami Y, Ikeda E, Jinzaki M, et al. Computed tomographic attenuation value of coronary atherosclerotic plaques with different tube voltage: an ex vivo study. Journal of computer assisted tomography. 2010; 34:58–63. [PubMed: 20118723]
25. Obaid DR, Calvert PA, Gopalan D, et al. Dual-energy computed tomography imaging to determine atherosclerotic plaque composition: a prospective study with tissue validation. Journal of cardiovascular computed tomography. 2014; 8:230–7. [PubMed: 24939072]
26. Henzler T, Porubsky S, Kayed H, et al. Attenuation-based characterization of coronary atherosclerotic plaque: comparison of dual source and dual energy CT with single-source CT and histopathology. European journal of radiology. 2011; 80:54–9. [PubMed: 20810229]
27. Scheffel H, Alkadhi H, Plass A, et al. Accuracy of dual-source CT coronary angiography: First experience in a high pre-test probability population without heart rate control. European radiology. 2006; 16:2739–47. [PubMed: 17031451]
28. Sun G, Li M, Jiang ZW, et al. Diagnostic accuracy of dual-source CT coronary angiography in patients with atrial fibrillation: meta analysis. European journal of radiology. 2013; 82:1749–54. [PubMed: 23727381]
29. Scheske JA, O'Brien JM, Earls JP, et al. Coronary artery imaging with single-source rapid kilovolt peak-switching dual-energy CT. Radiology. 2013; 268:702–9. [PubMed: 23579045]
30. Yu L, Christner JA, Leng S, Wang J, Fletcher JG, McCollough CH. Virtual monochromatic imaging in dual-source dual-energy CT: radiation dose and image quality. Medical physics. 2011; 38:6371–9. [PubMed: 22149820]
31. So A, Hsieh J, Imai Y, et al. Prospectively ECG-triggered rapid kV-switching dual-energy CT for quantitative imaging of myocardial perfusion. JACC Cardiovascular imaging. 2012; 5:829–36. [PubMed: 22897997]
32. Bamberg F, Dierks A, Nikolaou K, Reiser MF, Becker CR, Johnson TR. Metal artifact reduction by dual energy computed tomography using monoenergetic extrapolation. European radiology. 2011; 21:1424–9. [PubMed: 21249370]

33. Boll DT, Merkle EM, Paulson EK, Fleiter TR. Coronary stent patency: dual-energy multidetector CT assessment in a pilot study with anthropomorphic phantom. Radiology. 2008; 247:687–95. [PubMed: 18424688]
34. Boll DT, Merkle EM, Paulson EK, Mirza RA, Fleiter TR. Calcified vascular plaque specimens: assessment with cardiac dual-energy multidetector CT in anthropomorphically moving heart phantom. Radiology. 2008; 249:119–26. [PubMed: 18710959]
35. Stehli J, Fuchs TA, Singer A, et al. First experience with single-source, dual-energy CCTA for monochromatic stent imaging. European heart journal cardiovascular Imaging. 2014
36. Secchi F, De Cecco CN, Spearman JV, et al. Monoenergetic extrapolation of cardiac dual energy CT for artifact reduction. Acta radiologica. 2014
37. Yamada M, Jinzaki M, Kuribayashi S, Imanishi N, Funato K, Aiso S. Beam-hardening correction for virtual monochromatic imaging of myocardial perfusion via fast-switching dual-kVp 64-slice computed tomography: a pilot study using a human heart specimen. Circulation journal : official journal of the Japanese Circulation Society. 2012; 76:1799–801. [PubMed: 22664799]
38. So A, Lee TY, Imai Y, et al. Quantitative myocardial perfusion imaging using rapid kVp switch dual-energy CT: preliminary experience. Journal of cardiovascular computed tomography. 2011; 5:430–42. [PubMed: 22146502]
39. So A, Lee TY. Quantitative myocardial CT perfusion: a pictorial review and the current state of technology development. Journal of cardiovascular computed tomography. 2011; 5:467–81. [PubMed: 22146506]
40. Matsumoto K, Jinzaki M, Tanami Y, Ueno A, Yamada M, Kuribayashi S. Virtual monochromatic spectral imaging with fast kilovoltage switching: improved image quality as compared with that obtained with conventional 120-kVp CT. Radiology. 2011; 259:257–62. [PubMed: 21330561]
41. Leipsic J, LaBounty TM, Mancini GB, et al. A prospective randomized controlled trial to assess the diagnostic performance of reduced tube voltage for coronary CT angiography. AJR American journal of roentgenology. 2011; 196:801–6. [PubMed: 21427328]
42. Menke J, Unterberg-Buchwald C, Staab W, Sohns JM, Seif Amir Hosseini A, Schwarz A. Head-to-head comparison of prospectively triggered vs retrospectively gated coronary computed tomography angiography: Meta-analysis of diagnostic accuracy, image quality, and radiation dose. American heart journal. 2013; 165:154–63. e3. [PubMed: 23351817]
43. Sun Z, Ng KH. Prospective versus retrospective ECG-gated multislice CT coronary angiography: a systematic review of radiation dose and diagnostic accuracy. European journal of radiology. 2012; 81:e94–100. [PubMed: 21316887]
44. Hausleiter J, Meyer T, Hadamitzky M, et al. Radiation dose estimates from cardiac multislice computed tomography in daily practice: impact of different scanning protocols on effective dose estimates. Circulation. 2006; 113:1305–10. [PubMed: 16520411]
45. Kerl JM, Bauer RW, Maurer TB, et al. Dose levels at coronary CT angiography--a comparison of Dual Energy-, Dual Source- and 16-slice CT. European radiology. 2011; 21:530–7. [PubMed: 20862476]
46. Halliburton SS, Sola S, Kuzmiak SA, et al. Effect of dual-source cardiac computed tomography on patient radiation dose in a clinical setting: comparison to single-source imaging. Journal of cardiovascular computed tomography. 2008; 2:392–400. [PubMed: 19083984]
47. Raju R, Thompson AG, Lee K, et al. Reduced iodine load with CT coronary angiography using dual-energy imaging: a prospective randomized trial compared with standard coronary CT angiography. Journal of cardiovascular computed tomography. 2014; 8:282–8. [PubMed: 25151920]
48. Achenbach S, Marwan M, Schepis T, et al. High-pitch spiral acquisition: a new scan mode for coronary CT angiography. Journal of cardiovascular computed tomography. 2009; 3:117–21. [PubMed: 19332343]
49. Lell M, Marwan M, Schepis T, et al. Prospectively ECG-triggered high-pitch spiral acquisition for coronary CT angiography using dual source CT: technique and initial experience. European radiology. 2009; 19:2576–83. [PubMed: 19760421]

50. Achenbach S, Goroll T, Seltmann M, et al. Detection of coronary artery stenoses by low-dose, prospectively ECG-triggered, high-pitch spiral coronary CT angiography. JACC Cardiovascular imaging. 2011; 4:328–37. [PubMed: 21492807]
51. Achenbach S, Marwan M, Ropers D, et al. Coronary computed tomography angiography with a consistent dose below 1 mSv using prospectively electrocardiogram-triggered high-pitch spiral acquisition. European heart journal. 2010; 31:340–6. [PubMed: 19897497]
52. Alkadhi H, Stolzmann P, Desbiolles L, et al. Low-dose, 128-slice, dual-source CT coronary angiography: accuracy and radiation dose of the high-pitch and the step-and-shoot mode. Heart. 2010; 96:933–8. [PubMed: 20538669]
53. Gordic S, Husarik DB, Desbiolles L, Leschka S, Frauenfelder T, Alkadhi H. High-pitch coronary CT angiography with third generation dual-source CT: limits of heart rate. The international journal of cardiovascular imaging. 2014; 30:1173–9. [PubMed: 24816910]
54. Hell MM, Bittner D, Schuhbaeck A, et al. Prospectively ECG-triggered high-pitch coronary angiography with third-generation dual-source CT at 70 kVp tube voltage: feasibility, image quality, radiation dose, and effect of iterative reconstruction. Journal of cardiovascular computed tomography. 2014; 8:418–25. [PubMed: 25439789]
55. Leschka S, Stolzmann P, Desbiolles L, et al. Diagnostic accuracy of high-pitch dual-source CT for the assessment of coronary stenoses: first experience. European radiology. 2009; 19:2896–903. [PubMed: 19760229]
56. Morsbach F, Gordic S, Desbiolles L, et al. Performance of turbo high-pitch dual-source CT for coronary CT angiography: first ex vivo and patient experience. European radiology. 2014; 24:1889–95. [PubMed: 24838737]
57. Schuhbaeck A, Achenbach S, Layritz C, et al. Image quality of ultra-low radiation exposure coronary CT angiography with an effective dose <0. 1 mSv using high-pitch spiral acquisition and raw data-based iterative reconstruction. European radiology. 2013; 23:597–606. [PubMed: 22983283]
58. Yin WH, Lu B, Li N, et al. Iterative reconstruction to preserve image quality and diagnostic accuracy at reduced radiation dose in coronary CT angiography: an intraindividual comparison. JACC Cardiovascular imaging. 2013; 6:1239–49. [PubMed: 24269265]
59. Yin WH, Lu B, Hou ZH, et al. Detection of coronary artery stenosis with sub-milliSievert radiation dose by prospectively ECG-triggered high-pitch spiral CT angiography and iterative reconstruction. European radiology. 2013; 23:2927–33. [PubMed: 23807568]
60. Numburi UD, Schoenhagen P, Flamm SD, et al. Feasibility of dual-energy CT in the arterial phase: Imaging after endovascular aortic repair. AJR American journal of roentgenology. 2010; 195:486–93. [PubMed: 20651209]
61. Kaufmann S, Sauter A, Spira D, et al. Tin-filter enhanced dual-energy-CT: image quality and accuracy of CT numbers in virtual noncontrast imaging. Academic radiology. 2013; 20:596–603. [PubMed: 23490736]
62. Yamada Y, Jinzaki M, Okamura T, et al. Feasibility of coronary artery calcium scoring on virtual unenhanced images derived from single-source fast kVp-switching dual-energy coronary CT angiography. Journal of cardiovascular computed tomography. 2014; 8:391–400. [PubMed: 25301045]
63. Fuchs TA, Stehli J, Dougoud S, et al. Coronary artery calcium quantification from contrast enhanced CT using gemstone spectral imaging and material decomposition. The international journal of cardiovascular imaging. 2014; 30:1399–405. [PubMed: 24993390]
64. Moos SI, van Vemde DN, Stoker J, Bipat S. Contrast induced nephropathy in patients undergoing intravenous (IV) contrast enhanced computed tomography (CECT) and the relationship with risk factors: a meta-analysis. European journal of radiology. 2013; 82:e387–99. [PubMed: 23711425]
65. Yamamuro M, Tadamura E, Kanao S, et al. Coronary angiography by 64-detector row computed tomography using low dose of contrast material with saline chaser: influence of total injection volume on vessel attenuation. Journal of computer assisted tomography. 2007; 31:272–80. [PubMed: 17414766]
66. Dilmanian FA, Wu XY, Parsons EC, et al. Single-and dual-energy CT with monochromatic synchrotron x-rays. Physics in medicine and biology. 1997; 42:371–87. [PubMed: 9044419]

67. Grant KL, Flohr TG, Krauss B, Sedlmair M, Thomas C, Schmidt B. Assessment of an advanced image-based technique to calculate virtual monoenergetic computed tomographic images from a dual-energy examination to improve contrast-to-noise ratio in examinations using iodinated contrast media. Investigative radiology. 2014; 49:586–92. [PubMed: 24710203]
68. Carrascosa P, Capunay C, Rodriguez-Granillo GA, Deviggiano A, Vallejos J, Leipsic JA. Substantial iodine volume load reduction in CT angiography with dual-energy imaging: insights from a pilot randomized study. The international journal of cardiovascular imaging. 2014; 30:1613–20. [PubMed: 25053514]
69. Cormode DP, Naha PC, Fayad ZA. Nanoparticle contrast agents for computed tomography: a focus on micelles. Contrast media & molecular imaging. 2014; 9:37–52. [PubMed: 24470293]
70. Peer D, Karp JM, Hong S, Farokhzad OC, Margalit R, Langer R. Nanocarriers as an emerging platform for cancer therapy. Nature nanotechnology. 2007; 2:751–60.
71. van Schooneveld MM, Cormode DP, Koole R, et al. A fluorescent, paramagnetic and PEGylated gold/silica nanoparticle for MRI, CT and fluorescence imaging. Contrast media & molecular imaging. 2010; 5:231–6. [PubMed: 20812290]
72. Torchilin VP, Frank-Kamenetsky MD, Wolf GL. CT visualization of blood pool in rats by using long-circulating, iodine-containing micelles. Academic radiology. 1999; 6:61–5. [PubMed: 9891154]
73. Trubetskoy VS, Gazelle GS, Wolf GL, Torchilin VP. Block-copolymer of polyethylene glycol and polylysine as a carrier of organic iodine: design of long-circulating particulate contrast medium for X-ray computed tomography. Journal of drug targeting. 1997; 4:381–8. [PubMed: 9239578]
74. Kinsella JM, Jimenez RE, Karmali PP, et al. X-ray computed tomography imaging of breast cancer by using targeted peptide-labeled bismuth sulfide nanoparticles. Angewandte Chemie. 2011; 50:12308–11. [PubMed: 22028313]
75. Cormode DP, Roessl E, Thran A, et al. Atherosclerotic plaque composition: analysis with multicolor CT and targeted gold nanoparticles. Radiology. 2010; 256:774–82. [PubMed: 20668118]
76. Cormode DP, Skajaa T, van Schooneveld MM, et al. Nanocrystal core high-density lipoproteins: a multimodality contrast agent platform. Nano letters. 2008; 8:3715–23. [PubMed: 18939808]
77. Hyafil F, Cornily JC, Feig JE, et al. Noninvasive detection of macrophages using a nanoparticulate contrast agent for computed tomography. Nature medicine. 2007; 13:636–41.
78. Hyafil F, Cornily JC, Rudd JH, Machac J, Feldman LJ, Fayad ZA. Quantification of inflammation within rabbit atherosclerotic plaques using the macrophage-specific CT contrast agent N1177: a comparison with 18F-FDG PET/CT and histology. Journal of nuclear medicine : official publication, Society of Nuclear Medicine. 2009; 50:959–65.
79. Rabin O, Manuel Perez J, Grimm J, Wojtkiewicz G, Weissleder R. An X-ray computed tomography imaging agent based on long-circulating bismuth sulphide nanoparticles. Nature materials. 2006; 5:118–22.
80. Pan D, Schirra CO, Senpan A, et al. An early investigation of ytterbium nanocolloids for selective and quantitative “multicolor” spectral CT imaging. ACS nano. 2012; 6:3364–70. [PubMed: 22385324]
81. Schlomka JP, Roessl E, Dorscheid R, et al. Experimental feasibility of multi-energy photon-counting K-edge imaging in pre-clinical computed tomography. Physics in medicine and biology. 2008; 53:4031–47. [PubMed: 18612175]
82. Ronaldson JP, Zainon R, Scott NJ, et al. Toward quantifying the composition of soft tissues by spectral CT with Medipix3. Medical physics. 2012; 39:6847–57. [PubMed: 23127077]
83. He P, Yu H, Thayer P, et al. Preliminary experimental results from a MARS Micro-CT system. Journal of X-ray science and technology. 2012; 20:199–211. [PubMed: 22635175]
84. Iwanczyk JS, Nygard E, Meirav O, et al. Photon Counting Energy Dispersive Detector Arrays for X-ray Imaging. IEEE transactions on nuclear science. 2009; 56:535–542. [PubMed: 19920884]
85. Kappler S, Hannemann T, Kraft E, et al. First results from a hybrid prototype CT scanner for exploring benefits of quantum-counting in clinical CT. Proc Spie. 2012:8313.
86. Taguchi K, Iwanczyk JS. Vision 20/20: Single photon counting x-ray detectors in medical imaging. Medical physics. 2013; 40:100901. [PubMed: 24089889]

87. Feuerlein S, Roessl E, Proksa R, et al. Multienergy photon-counting K-edge imaging: potential for improved luminal depiction in vascular imaging. Radiology. 2008; 249:1010–6. [PubMed: 18849505]

88. Boussel L, Coulon P, Thran A, et al. Photon counting spectral CT component analysis of coronary artery atherosclerotic plaque samples. The British journal of radiology. 2014; 87:20130798. [PubMed: 24874766]

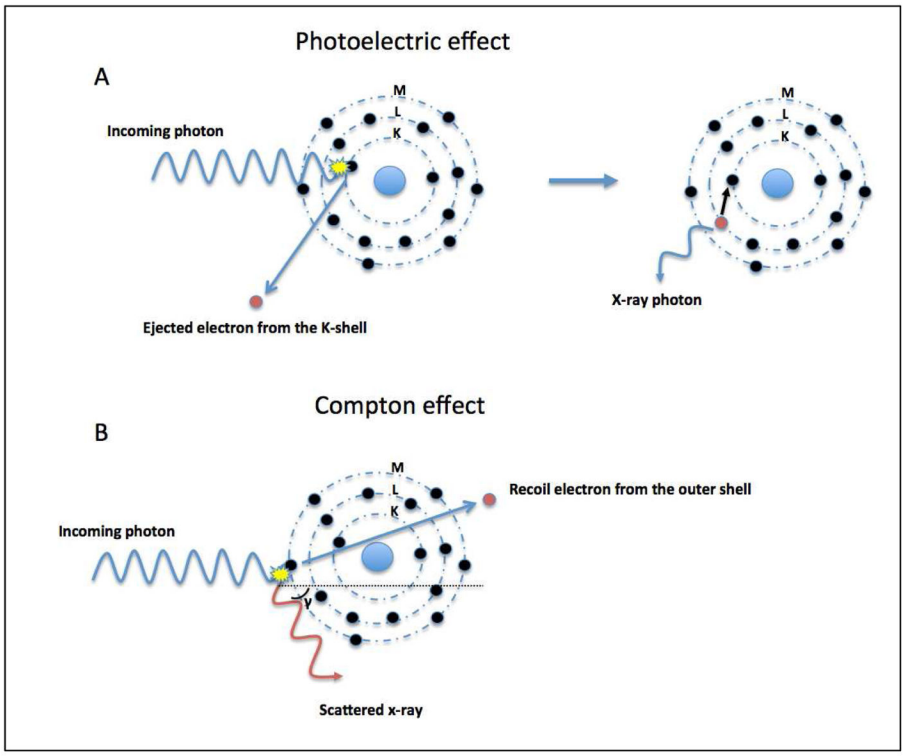

Figure 1. Schematic illustration of the photoelectric (A) and Compton (B) effect

Photoelectric effect (**A**): An incoming photon collides with an electron and its energy is totally absorbed. If the kinetic energy of the photon is greater than the binding energy of the electron this will result in its ejection out of the K-shell (innermost shell of an atom). An electron from another layer moves to occupy the vacancy left in the inner layer by the ejected electron. This transition is accompanied by the release of x-ray photons.

Compton effect (**B**): This is a radiation scattering event, whereby the incoming x-ray photon ejects an electron from the outermost shell of an atom and is scattered. Due to its loss of kinetic energy, the wavelength of the incoming photon becomes longer and the photon can become red shifted (red light has the longest wavelength).

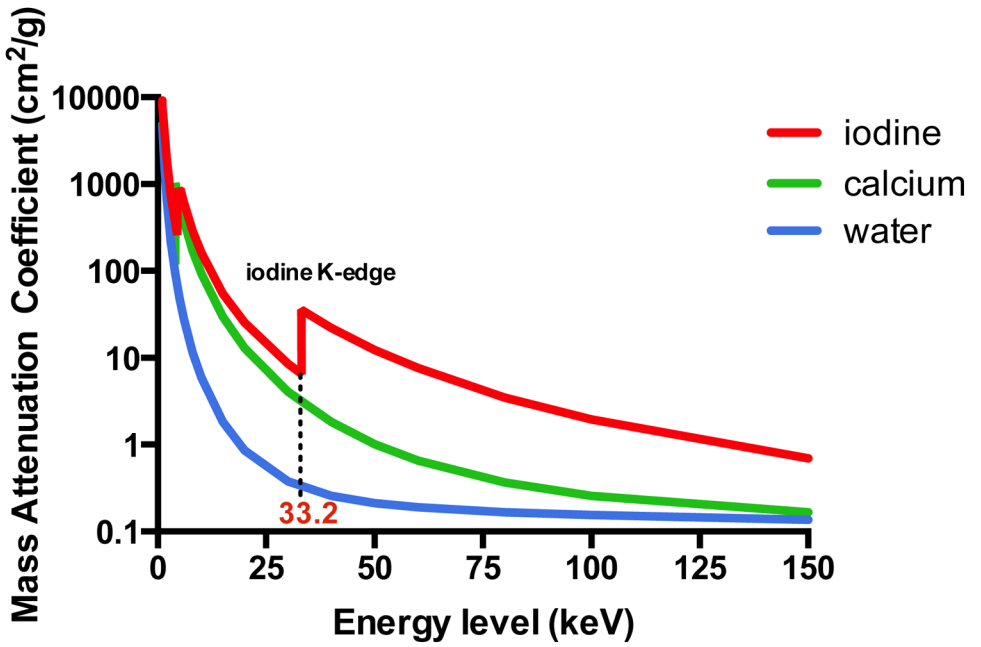

Figure 2. Mass-attenuation coefficients for iodine (red), calcium (green), and water (blue) at different photon energies

Please note the attenuation peak of iodine (Z=53) at 33 keV. This peak represents the k-edge of iodine.

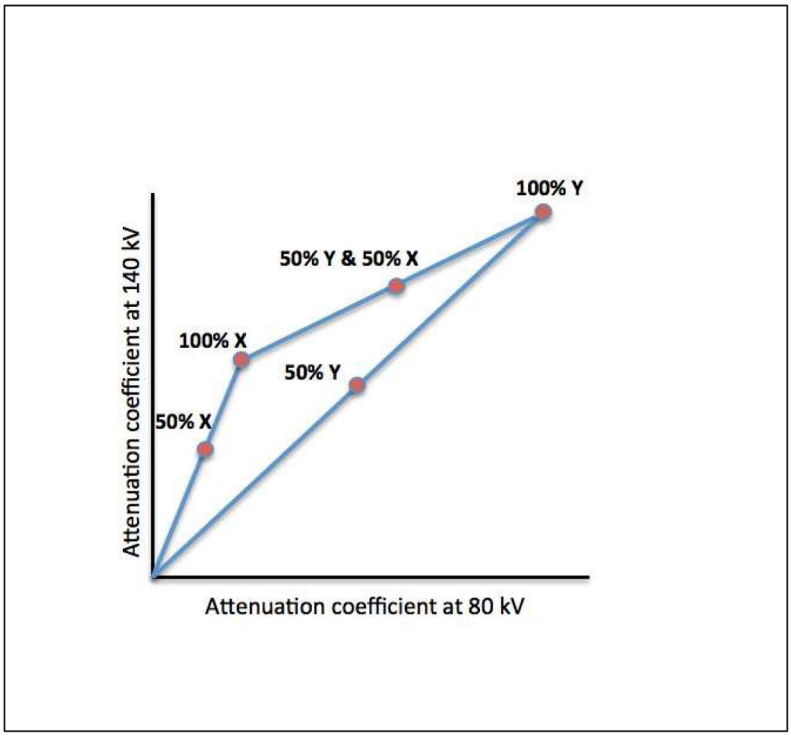

Figure 3. Linear attenuation coefficients of materials X and Y

With dual-energy computed tomography, unknown materials are reflected as a composition of basis materials X and Y.

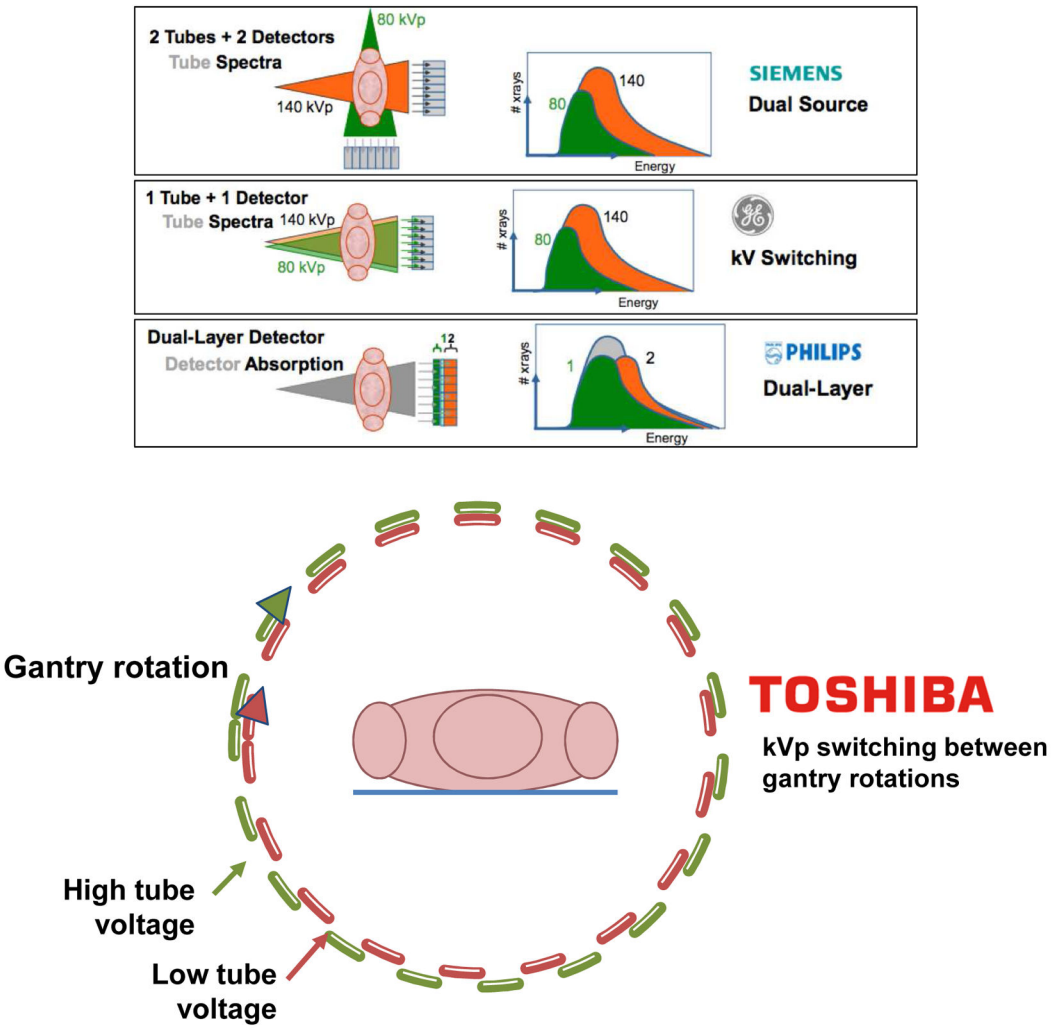

Figure 4. Schematic illustration of four different approaches for obtaining dual-energy information (Courtesy of Philips Healthcare, Best, The Netherlands)

(**A**) Dual source-detector pairs with each source operating at a different tube voltage. Each x-ray source covers a different scan field. (**B**) Single source-detector pair with the source capable of rapid voltage switching in a single gantry rotation. (**C**) Single source-detector pair with a dual-layer detector made of two different materials capable of differentiating between low (upper layer) and high-energy photons (bottom layer) with the source operating at constant tube voltage. (**D**) Single source detector pair with tube voltage switching between sequential gantry rotations.

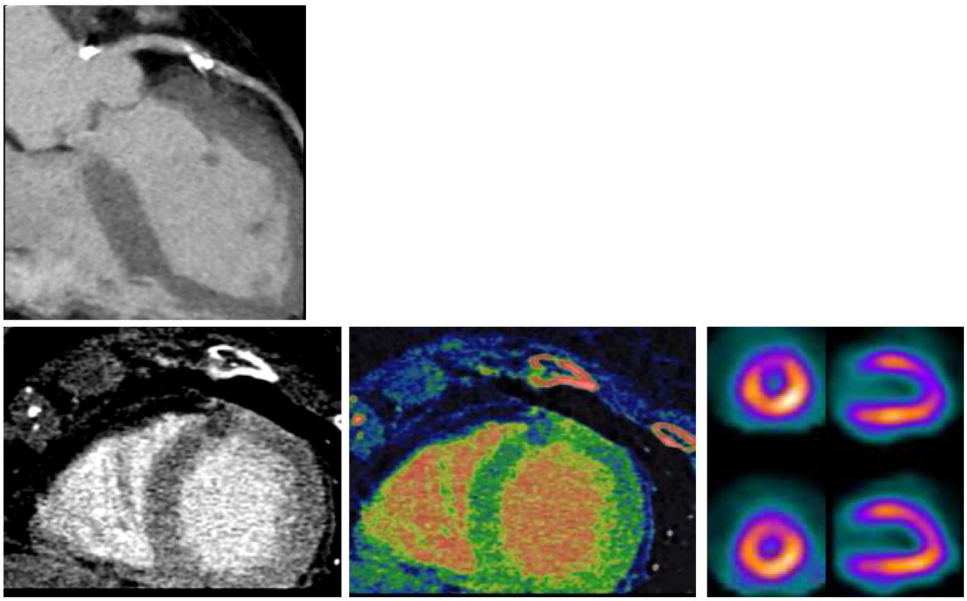

Figure 5. A 77-year old woman with hypertension, hypercholesterolemia, and atypical angina chest pain

(**A**) Curved MPR of the left anterior descending artery shows a calcified plaque with significant stenosis. (**B–D**) Both assessment of CT perfusion (**B**) myocardial blood flow map (**C**) revealed an anterior perfusion defect (arrow, B and C), which was confirmed by SPECT (arrow, **D**).

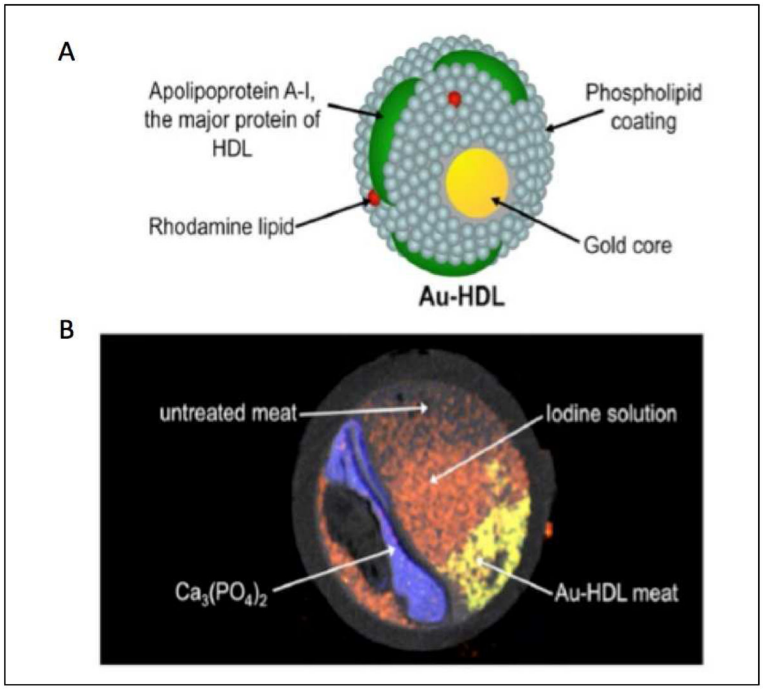

Figure 6. A gold based nanoparticle and spectral CT for atherosclerotic plaque composition

(A) Structure of a CT gold-high-density-lipoprotein (HDL) nanoparticle contrast agent targeted at macrophages. (B) Spectral CT image of a phantom model of an artery using gold nanoparticles. Adapted from Cormode et al (reference 43) with permission of the publisher.

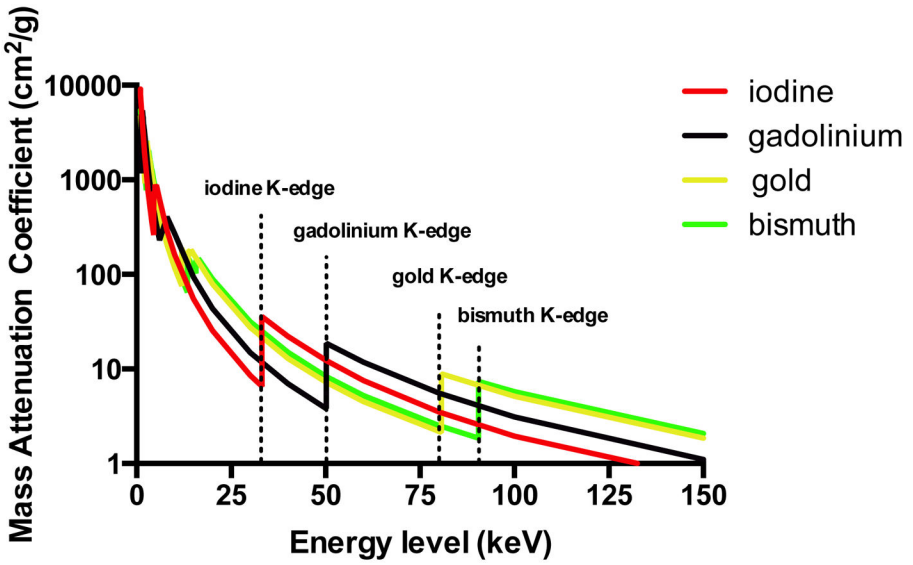

Figure 7. Mass-attenuation coefficients for iodine (red), gadolinium (black), gold (yellow), and bismuth (green) at different photon energies

The lower energy photons of the spectrum are almost totally absorbed by surrounding tissues, rendering K-edge imaging using iodine contrast agents a challenging task.